Journal of Power Sources 212 (2012) 93–99

Contents lists available at SciVerse ScienceDirect

Journal of Power Sources

journal homepage: www.elsevier.com/locate/jpowsour

Short communication

Effect of spatial variation of gas diffusion layer wetting characteristics on through-plane water distribution in a polymer electrolyte fuel cell

Kyungmun Kang, Kyeongmin Oh, Sunghyun Park, Arae Jo, Hyunchul Ju*

School of Mechanical Engineering, Inha University, 253 Yonghyun-Dong, Nam-Gu, Incheon 402-751, Republic of Korea

ARTICLE INFO

Article history:
Received 31 January 2012
Received in revised form
14 March 2012
Accepted 17 March 2012
Available online 10 April 2012

Keywords:
Polymer electrolyte fuel cell
Gas diffusion layer
Polytetrafluoroethylene (PTFE)
Through-plane water profile
Numerical simulation

ABSTRACT

Through-plane liquid water distributions recently visualized by Manahan et al. [1] and Turhan et al. [2] using the neutron radiography (NR) technique show that the peaks of the water distributions are located near the center of a gas diffusion layer (GDL). We suggest that the distinctive water profiles are caused by incomplete polytetrafluoroethylene (PTFE) treatment of the GDL and the resultant spatial variation of GDL wettability in the through-plane direction. Based on this hypothesis, we improve the macroscopic two-phase fuel cell model to describe two-phase transport through GDLs with variation of spatial wettability [3]. The proposed model successfully reproduces the shape of through-plane water profiles obtained from the NR experiments [1,2]. Therefore, the centrally located liquid saturation peak in the GDL can be attributed to incomplete PTFE treatment of the GDL. This occurs because liquid water is more easily accumulated in the relatively hydrophilic GDL pores encountered in the inner GDL region (rather than the outer GDL region) due to its incomplete PTFE treatment. Our results indicate that the overall characteristics of liquid water distribution in a GDL under an inhomogeneous wetting condition can be macroscopically predicted using the two-phase model presented here.

1. Introduction

A gas diffusion layer (GDL), usually made of carbon paper or carbon cloth, plays a crucial role in the water management of polymer electrolyte fuel cells (PEFCs). Because the carbon paper and carbon cloth GDL materials inherently exhibit hydrophilic behavior, they are treated with wet-proofing agents such as polytetrafluoroethylene (PTFE) to more efficiently remove product water during PEFC operation. However, after the wet-proofing treatment, the PTFE loading may not be uniform throughout the GDL due to the complex pore structure of the GDL [4]. Furthermore, a gradual loss of GDL hydrophobicity due to GDL aging also exists as reported in the literature [5,6].

Recently, Manahan et al. [1] and Turhan et al. [2] used the neutron radiography (NR) technique to visualize through-plane water profiles along the thickness of a GDL. As shown in Fig. 1, their NR data show that the peaks of the water distributions are all located near the center of the GDL thickness. Assuming uniform GDL properties, they concluded that this trend resulted from a combined effect of capillary flow and phase change-induced (PCI) flow. However, we emphasize that this type of water profile can be obtainable solely by capillary action, as long as porous properties such as porosity and contact angle are spatially non-uniform inside the GDL. Pore-scale simulation results described in the literature demonstrate that the spatial wettability variation throughout a GDL significantly alters capillary transport and the resultant water profile inside the GDL [7].

Previously, we developed a two-phase fuel cell model in which a new feature regarding the effect of the spatial variation of the GDL porous properties was modeled and implemented [3]. From our simulation results, we found that the wettability variation through the GDL thickness considerably altered the water transport characteristics and resultant water distribution in the GDL. The present study is an extension of our previous work [3], with the goal of reproducing the shape of through-plane water profiles obtained by Manahan et al. [1] and Turhan et al. [2]. By reasonably assuming the wetting property (contact angle) variation along the GDL thickness, our simulation results clearly demonstrate that a water peak can exist near the center of the GDL solely driven by capillary transport.

2. Numerical model

2.1. Two-phase fuel cell model

The one-dimensional (1-D) two-phase model presented in our previous study [3] was used to predict the experimental liquid

* Corresponding author. Tel.: +1 82 32 860 7312; fax: +1 82 32 868 1716.
E-mail address: hcju@inha.ac.kr (H. Ju).

0378-7753/$ – see front matter © 2012 Elsevier B.V. All rights reserved.
doi:10.1016/j.jpowsour.2012.03.058

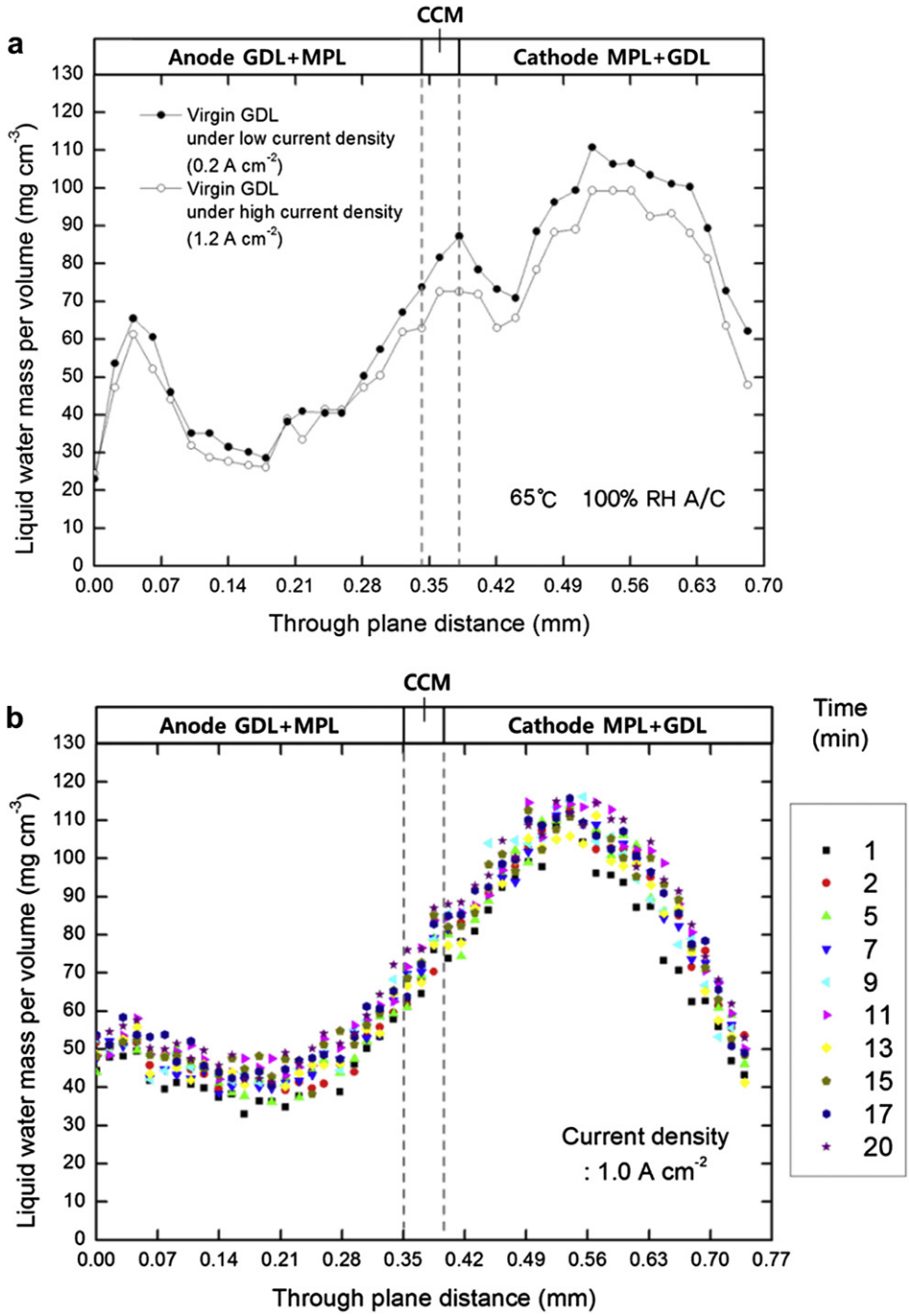

Fig. 1. NR data for through-plane liquid water distributions in the anode and cathode GDLs. Data were replotted from (a) Manahan et al. [1] (SGL 10BB type GDL with 250 μm thickness; active area, $A_{mem} = 5$ cm^2; cell temperature, $T_{cell} = 65$ °C; anode and cathode inlet humidification, $RH_a/RH_c = 100\%$; anode and cathode stoichiometric ratios, $\xi_a/\xi_c = 2.0/2.0$) and (b) Turhan et al. [2] (SGL 10BB type GDL with 300 μm thickness; active area, $A_{mem} = 17.2$ cm^2; anode and cathode inlet pressures, $P_a/P_c = 1$ atm; anode and cathode inlet humidification, $RH_a/RH_c = 100\%$; anode and cathode stoichiometric ratios, $\xi_a/\xi_c = 1.5/2.0$).

water profile through the GDL thickness. The model is based on a multiphase mixture (M^2) approach, and considers the effects of immobile liquid saturation and the spatial variation of GDL wettability on the liquid water distribution inside a GDL. The computational domain for the model includes the anode GDL, the catalyst-coated membrane (CCM), and the cathode GDL. Therefore, gas channels (GCs) and bipolar plates (BPs) for both the anode and cathode sides are excluded to simplify numerical analysis. Regarding the water transport across the membrane, all three modes comprising the hydraulic pressure gradient, the membrane water content gradient, and the electro-osmotic drag due to proton flux were rigorously taken into account for a more accurate prediction of water transport and accumulation inside a cell. The computational domain and the transport processes for the present model are schematically shown in Fig. 2.

2.2. Governing and constitutive equations

The present two-phase model is governed by conservation of mass, momentum, and species. All the governing equations of this

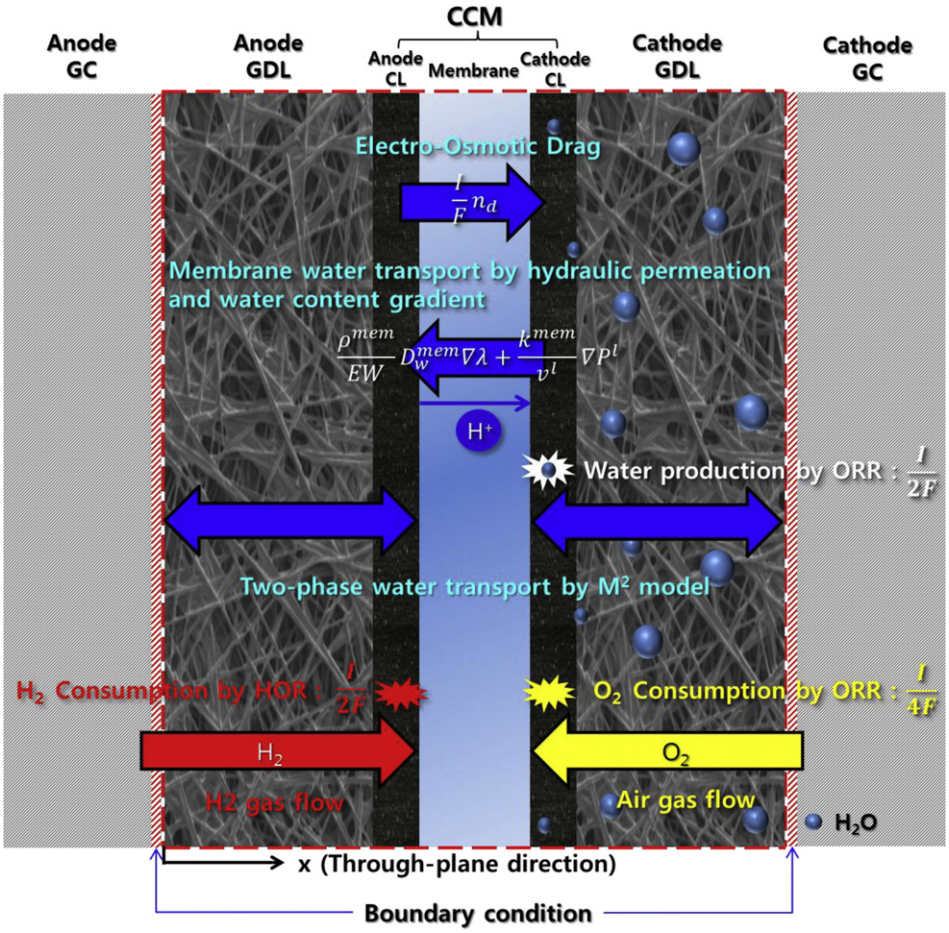

Fig. 2. Schematic of computational domain (red dashed line) and electrochemical reactions/transport phenomena considered in the model. HOR and ORR denote hydrogen oxidation reaction in anode side and oxygen reduction reaction in the cathode side, respectively (For interpretation of the references to colour in this figure legend, the reader is referred to the web version of this article.).

model are listed in Table 1. Additionally, the transport properties in the membrane and the cell design/material/physical properties are summarized in Tables 2 and 3, respectively. Readers are referred to Ju [3] for more detailed elaboration of the model. Since the focus of the present study is on water transport through GDLs with variation of spatial wettability, the water transport equation for this type of GDL is described here in more detail.

The steady state 1-D water conservation equation in the through-plane direction (x) can be written as [3]

$$\frac{\mathrm{d}}{\mathrm{d}x}(\gamma_{\mathrm{w}}\rho m_{\mathrm{w}}u) = \frac{\mathrm{d}}{\mathrm{d}x}\left[\rho^{\mathrm{g}} D_{\mathrm{w}}^{\mathrm{g,eff}} \frac{\mathrm{d}}{\mathrm{d}x}(m_{\mathrm{w}}^{\mathrm{g}})\right] + \frac{\mathrm{d}}{\mathrm{d}x}\left[\left(m_{\mathrm{w}}^{\mathrm{g}} - m_{\mathrm{w}}^{\mathrm{l}}\right) j^{\mathrm{l}}\right] \quad (12)$$

It should be noted that in the M^2 model, a diffusive mass flux of each phase relative to the whole multiphase mixture is defined, and j^{l} in the second term on the right-hand side of Eq. (12) denotes the diffusive mass flux of the liquid phase relative to the whole multiphase mixture as follows [11]:

$$j^{\mathrm{l}} = \rho^{\mathrm{l}} u^{\mathrm{l}} - \lambda^{\mathrm{l}} \rho u \quad (13)$$

Therefore, the second term on the right-hand side of Eq. (12) (i.e. the capillary transport term) is due to the relative motion between the gas and liquid phases and is proportional to the capillary pressure gradient as follows:

$$\left(m_{\mathrm{w}}^{\mathrm{l}} - m_{\mathrm{w}}^{\mathrm{g}}\right)\vec{j}^{\mathrm{l}} = \left(1 - m_{\mathrm{w}}^{\mathrm{g}}\right)\frac{K}{\nu}\lambda^{\mathrm{l}}\lambda^{\mathrm{g}}\frac{\mathrm{d}P_c}{\mathrm{d}x} \quad (14)$$

In Eq. (14), the capillary pressure P_c, which is defined as the difference between the gas and liquid pressures, is expressed as [3]

$$P_c = P^{\mathrm{g}} - P^{\mathrm{l}} = \sigma\cos\theta\left(\frac{\varepsilon}{K}\right)^{1/2} J(s_r) \quad (15)$$

where ε, K, and θ are the porosity, permeability, and contact angle of the given porous GDL, respectively. The Leverett function, $J(s_r)$, which is a dimensionless capillary pressure, can be expressed as a function of the liquid saturation s_r for the given hydrophobic GDL as follows:

$$J\left(s_r\right) = \begin{cases} 0 & \text{if } s_r \le s_{\mathrm{im}} \\ 1.417s_r - 2.120s_r^2 + 1.263s_r^3 & \text{if } s_r > s_{\mathrm{im}} \end{cases} \quad (16)$$

In Eq. (16), s_{im} is the immobile liquid saturation and s_r is the liquid saturation representing the volume fraction of GDL pores occupied by transportable liquid as follows:

$$s_r = \frac{V^{\mathrm{l}}/V_{\mathrm{pore}} - s_{\mathrm{im}}}{1 - s_{\mathrm{im}}} \quad (17)$$

It should be emphasized here that the standard Leverett J-function form in Eq. (16) was formulated to characterize the liquid transport in more uniform porous media such as soils and rocks [12,13]. A more realistic capillary pressure-saturation study focusing on real fuel cell GDL was conducted by Gostick et al. [14] and Kumbur et al. [15,16]. In particular, Kumbur et al. [15,16] conducted capillary pressure-saturation measurements under typical

Table 1
Governing equations of the 1-D two-phase fuel cell model.

	Governing equations
Mass	For the anode GDL:
	$\rho u = \frac{I}{2F}M_{H_2} + \left[n_d\frac{I}{F} - D_w^{mem}\frac{\rho^{mem}}{EW}\left(\frac{d\lambda}{dx}\right)_{mem}\right]M_w - \frac{K^{mem}}{\nu^l}\left(\frac{dP^l}{dx}\right)_{mem}$ (1)
	For the cathode GDL:
	$\rho u = -\frac{I}{4F}M_{O_2} + \frac{I}{2F}M_w + \left[\left(n_d+\frac{1}{2}\right)\frac{I}{F} - D_w^{mem}\frac{\rho^{mem}}{EW}\left(\frac{d\lambda}{dx}\right)_{mem}\right]M_w - \frac{K^{mem}}{\nu^l}\left(\frac{dP^l}{dx}\right)_{mem}$ (2)
Momentum	For the anode and cathode GDLs:
	$\rho u = \frac{K}{\nu}\frac{dP}{dx}$ (3)
Species	Water transport in the anode GDL:
	$\gamma_w \rho m_w u = \rho^g D_w^{g,eff}\frac{d}{dx}(m_w^g) + \left(m_w^g - m_w^l\right)j^l + \left[n_d\frac{I}{F} - D_w^{mem}\frac{\rho^{mem}}{EW}\left(\frac{d\lambda}{dx}\right)_{mem}\right]M_w - \frac{K^{mem}}{\nu^l}\left(\frac{dP^l}{dx}\right)_{mem}$ (4)
	Water transport in the cathode GDL:
	$\gamma_w \rho m_w u = \rho^g D_w^{g,eff}\frac{d}{dx}(m_w^g) + \left(m_w^g - m_w^l\right)j^l + \left[\left(n_d+\frac{1}{2}\right)\frac{I}{F} - D_w^{mem}\frac{\rho^{mem}}{EW}\left(\frac{d\lambda}{dx}\right)_{mem}\right]M_w - \frac{K^{mem}}{\nu^l}\left(\frac{dP^l}{dx}\right)$ (5)
	Water transport across the membrane:
	$\frac{d}{dx}\left(\frac{\rho^{mem}}{EW}D_w^{mem}\frac{d\lambda}{dx}\right)M_w - \frac{d}{dx}\left(n_d\frac{I}{F}\right)M_w + \frac{d}{dx}\left(\frac{K^{mem}}{\nu^l}\frac{dP^l}{dx}\right) = 0$ (6)
	Oxygen transport in cathode GDL:
	$\gamma_{O_2}\rho m_{O_2} u = \rho^g D_{O_2}^{g,eff}\frac{d}{dx}\left(m_{O_2}^g\right) + m_{O_2}^g j^l - \frac{I}{4F}M_{O_2}$ (7)

fuel cell compressed GDL and operating temperatures (20, 50, and 80 °C). They compared their experimental measurements and capillary pressure-saturation correlation test data obtained with the traditional Leverett function. According to their comparison, the deviation between the Leverett function and new correlations is not significant, especially for the practical range of liquid saturation ($0 < s < 0.5$) in GDL during fuel cell operation. Therefore, we employ the standard Leverett J-function, i.e. Eq. (16), for this study.

Eq. (14) shows that capillary pressure P_c is a basic parameter characterizing liquid water transport in a porous GDL. By substituting the capillary pressure-related terms in Eqs. (15)–(17) into Eq. (14), the final form of the capillary transport term described by Eq. (14) can be written as follows:

$$\left(m_w^l - m_w^g\right)\vec{j}^l = \left(1 - m_w^g\right)\frac{\lambda^l\lambda^g\sigma(\varepsilon K)^{1/2}}{\nu}\left[\cos\theta\frac{dJ}{ds_r}\frac{ds_r}{dx} + J(s_r)\frac{d(\cos\theta)^{1/2}}{dx}\right] \quad (18)$$

where the first and second terms on the right-hand side of Eq. (18) represent capillary transport driven by the liquid saturation gradient and the spatial variation of the GDL wetting characteristic (contact angle θ), respectively. It should be emphasized that the second term on the right-hand side of Eq. (18) is the distinctive feature of the proposed model and is necessary to describe two-phase transport through a porous medium with inhomogeneous surface wettability. However, the second term is not included in most macroscopic two-phase fuel cell models introduced in the literature.

2.3. Boundary conditions

As indicated in Fig. 2, the aforementioned one-dimensional model requires boundary conditions for water and oxygen species at the GC/GDL interfaces. The interfacial mass fractions for oxygen and water species, $m_{i,GDL/GC}$, are determined by the cell operating pressure (P), temperature (T), GC relative humidity (RH_{GC}), and interfacial liquid droplet coverage s_{int} due to channel flooding conditions.

$$m_{w,GDL/GC}(s_{int}, RH_{GC}, T, P) = \frac{\rho^l s_{int} + (1 - s_{int})\cdot\frac{P_w M_w}{R_u T}}{\rho^l s_{int} + \rho^g(1 - s_{int})} = \frac{\rho^l s_{int} + (1 - s_{int})\cdot\frac{RH_{GC}\cdot P_{sat}\cdot M_w}{R_u T}}{\rho^l s_{int} + \rho^g(1 - s_{int})} \quad (19)$$

Table 2
Transport properties of electrolyte phase.

Expression
Water activity [8]:
$a = \frac{C_w^g R_u T}{p^{sat}}$ (8)
Water content:
$\lambda = \begin{cases} \lambda^g = 0.043 + 17.81a - 39.85a^2 + 36.0a^3 & \text{for } 0 < a \le 1 \\ \lambda^l = 22 \end{cases}$ (9)
Electro-osmotic drag coefficient [9]:
$n_d = \begin{cases} 1 & \lambda \le \lambda^g \quad (a = 1) \\ 2.5 & \lambda = \lambda^l \end{cases}$ (10)
Water diffusion coefficient in the membrane ($m^2\ s^{-1}$) [10]:
$D_w^{mem} = \begin{cases} 3.1\times10^{-7}\lambda\left(e^{0.28\lambda} - 1\right)e^{(-2346/T)} & \text{for } 0 < \lambda \le 3 \\ 4.17\times10^{-8}\lambda\left(1 + 161e^{-\lambda}\right)e^{(-2346/T)} & \text{otherwise} \end{cases}$ (11)

Table 3
Cell design, material and physical parameters.

Description	Value
Porosity of the GDL, ε_{GDL}	0.6
Permeability of the GDL, K_{GDL}	1.0×10^{-12} m^2
Thickness of GDL, δ_{GDL}	0.3 mm
Hydraulic permeability of the membrane, K_{mem}	5.0×10^{-20} m^2
Thickness of membrane, δ_{mem}	0.018 mm
Dry membrane density, ρ_{mem}	2000 kg m^{-3}
Equivalent weight of electrolyte in the membrane, EW	1.1 kg mol^{-1}
Faraday constant, F	96,487 C mol^{-1}
Universal gas constant, R_u	8.314 J mol^{-1} K^{-1}
Surface tension, σ	0.0625 N m^{-1}
Liquid water density, ρ^l (80 °C)	972 kg m^{-3}
Liquid water viscosity, μ^l	3.5×10^{-4} N s m^{-2}

$$m_{O_2,GDL/GC}(s_{int}, RH, T, P) = \frac{(1-s_{int})M_{O_2}\frac{P_{O_2}}{R_u T}}{\rho^l s_{int} + \rho^g(1-s_{int})} = \frac{(1-s_{int})M_{O_2}\frac{P-P_w-P_{N_2}}{R_u T}}{\rho^l s_{int} + \rho^g(1-s_{int})} \quad (20)$$

2.4. Numerical procedures

The first order ordinary differential equations shown in Table 1 are solved separately in three different regions, i.e. anode GDL, CCM, and cathode GDL. 20 grid points for each of three computational regions was found to provide sufficient spatial resolution. In order to connect these differential equations for the three domains, an initial estimated value is provided for the water flux across the membrane to set up the interfacial boundary conditions. An iterative procedure is used to improve the initial estimate where the individually calculated interfacial fluxes in adjoining domains should be matched at the interface. The iterations proceed until the relative error falls below the convergence criterion (10^{-7}).

3. Results and discussion

We expected that the wetting characteristic of a GDL would vary spatially due to several possible reasons such as heterogeneous GDL pore structures, anomalies in the PTFE treatment, surface defects, impurities, and aging of the GDL. We focus on the effect of PTFE treatment on the liquid saturation profile. During PTFE treatment, a GDL is soaked in PTFE solution to enhance its water removal capability. As shown schematically in Fig. 3a, it is possible that the percolation of PTFE solution into a GDL (i.e. mainly driven by capillary effects) is not sufficient, causing fewer PTFE-coated pores near the center of a GDL than near the outer GDL region. Consequently, the center of a GDL can exhibit less hydrophobic behavior than the outer GDL surface, as shown in Fig. 3b. Recently, Rofaiel et al. [4] measured PTFE distributions in the through-plane direction for paper, felt, and cloth GDLs and their experimental data exhibit lower PTFE concentrations near the GDL core region as compared to the outer GDL surface for the paper and felt GDLs.

In our previous study [3], the effect of variation in GDL wettability along the GDL thickness was numerically investigated. Three

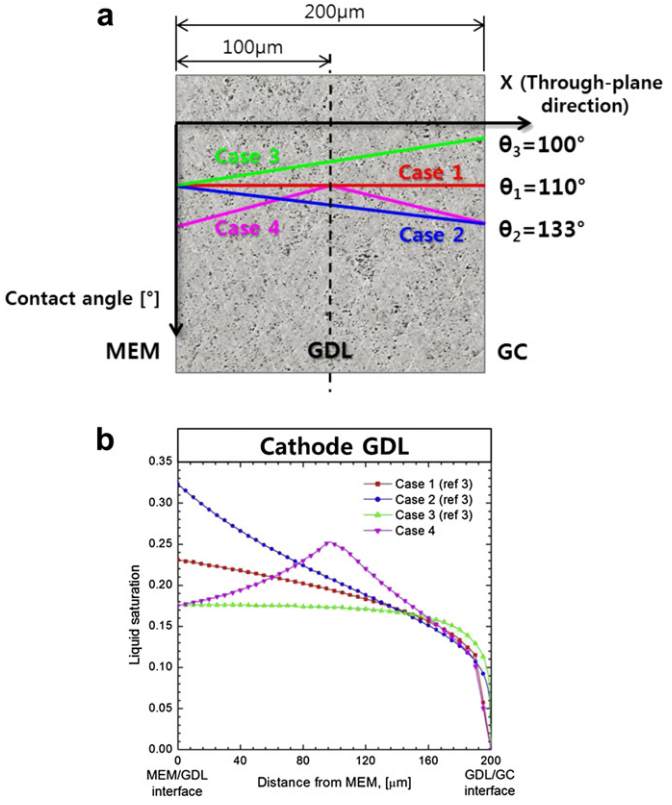

Fig. 4. (a) Schematic representation of spatial variation of the cathode GDL contact angle along the through-plane direction for Cases 1, 2, 3, and 4. (b) Comparison of calculated through-plane liquid saturation profiles in the cathode GDL. The simulation conditions were at 80 °C, 1.5 A cm^{-2}, and 1.5 atm for both anode and cathode GC inlet pressures.

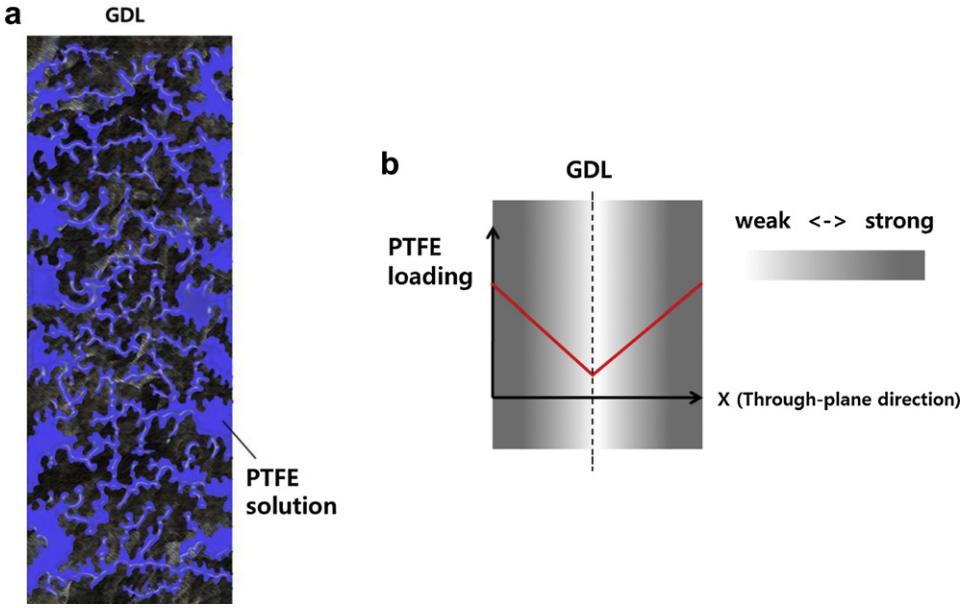

Fig. 3. (a) Schematic representation describing percolation of PTFE solution into a GDL during PTFE treatment process. (b) Possible variation of GDL wettability along the through-plane direction after PTFE treatment.

cases were defined by varying the cosine of the GDL contact angle (cos θ) along the GDL thickness. Case 1 is a reference case representing no variation of cos θ in the GDL thickness direction (i.e. a uniform contact angle) while the value of cos θ linearly increases (Case 2) or decreases (Case 3) from the CCM/GDL interface toward the GC. To analyze the effect of incomplete PTFE treatment, an additional case (Case 4) is newly defined and simulated in this study. As schematically described in Fig. 4a, the absolute value of cos θ for Case 4 decreases in the first half of the GDL and then increases again in the second half of the GDL.

Fig. 4b compares the calculated liquid saturation profile for Case 4 to those of Cases 1, 2, and 3. Since all four cases in Fig. 4b are based on the high current density fuel cell operation (1.5 A cm^{-2}), no liquid droplet coverage at the cathode GC/GDL interface is assumed due to the high gas flow rate in GCs and thus efficient droplet removal on the GDL surface [17,18]. The liquid saturation peak for Case 4 forms near the center of the GDL because liquid water accumulation is more strongly promoted by the relatively hydrophilic GDL inner region. The shape of the through-plane water distribution predicted by the proposed model qualitatively resembles the water profiles experimentally captured by Manahana et al. [1] and Turhan et al. [2] using the neutron imaging technique.

Fig. 5 shows the liquid saturation distributions of Case 4 at two different current densities of 0.2 A cm^{-2} and 1.2 A cm^{-2}. According to the experimental observations from Yang et al. [17] and Zhang et al. [18], the number of liquid droplets on the cathode GDL/GC interfacial surface is inversely proportional to the gas flow rate in GCs and thus operating current density. Therefore, we assume the values of interfacial droplet coverage at the cathode GDL/GC interface for the cases of 0.2 A cm^{-2} and 1.2 A cm^{-2} to be 15% and 7.5%, respectively. The liquid saturation peaks observed in these cases exists almost near the center of the GDL, which is driven by the assumed contact angle variation to approximate incomplete PTFE treatment (see Case 4 in Fig. 4a). More importantly, these two cases exhibit almost the same level of liquid saturation peak in the cathode GDL despite the significant difference in operating current density and thus water generation rate among these cases. The numerical trend is almost identical to the trend observed in the NR data measured by Manahana et al. [1] at 0.2 A cm^{-2} and 1.2 A cm^{-2} (see Fig. 1a).

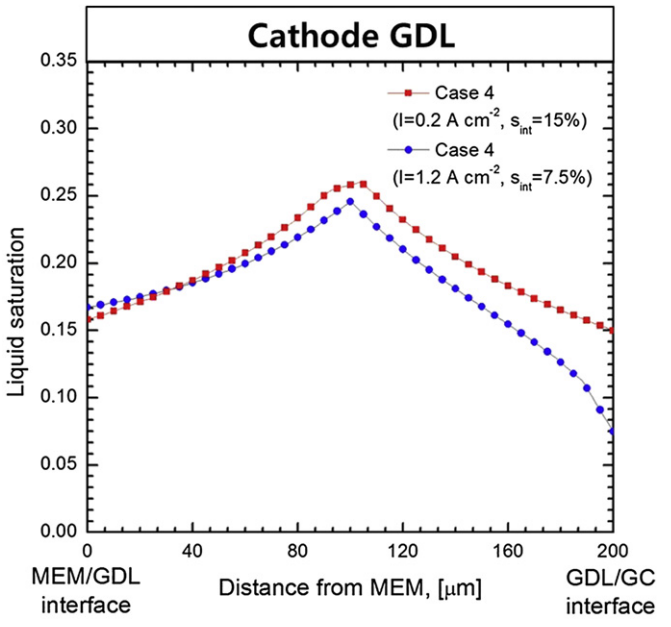

Fig. 5. Comparison of calculated through-plane liquid saturation profiles in the cathode GDL for case 4 at the two different current densities of 0.2 A cm^{-2} and 1.2 A cm^{-2}. The interfacial droplet coverage at the cathode GDL/GC, s_{int} is assumed to be 15% for the lower current density case (0.2 A cm^{-2}) and 7.5% for the higher current density case (1.2 A cm^{-2}). The simulation conditions were at 80 °C and 1.5 atm for both anode and cathode GC inlet pressures.

Our comparisons clearly indicate that an overall characteristic of liquid water transport through a GDL under inhomogeneous wetting and porous conditions can be macroscopically approximated by the proposed two-phase model with the consideration of contact angle dependence, i.e. the second term on the right-hand side of Eq. (18). This work successfully enhances the capability of a computational two-phase fuel cell model for a realistic prediction of the liquid water profile and flooding behavior in a GDL.

4. Conclusion and future plans

The through-plane water distributions in GDLs measured by Manahan et al. [1] and Turhan et al. [2] exhibit liquid saturation peaks near the centers of the GDLs. In this study, we demonstrated that the experimental trend observed in [1,2] was successfully captured by our macroscopic two-phase model in which we included the proposed term, i.e. the second term on the right-hand side of Eq. (18) describing two-phase transport through an inhomogeneous GDL with spatial variation of wettability. Our model simulation results indicate that the centrally located liquid saturation peaks in the GDLs can be attributed to relatively fewer PTFE-coated pores in the inner GDL region than in the outer GDL region due to incomplete PTFE treatment. Since the two-phase transport characteristic has a significant effect on GDL liquid saturation profiles and flooding behavior, efforts are currently underway to extend the present 1-D fuel cell model to a three-dimensional fuel cell model in order to more comprehensively study the phenomena.

Acknowledgments

This work was supported by a National Research Foundation of Korea (NRF) grant (no. NRF-2009-C1AAA001-2009-0093168) funded by the Ministry of Education, Science and Technology (MEST) of the Korean government. Hyunchul Ju acknowledges partial support from an Agency for Defense Development grant (no. UD090080GD).

Nomenclature

a	water activity or effective catalyst area per unit of total volume (m^2 m^{-3})
D_k	mass diffusivity of species k (m^2 s^{-1})
EW	equivalent weight of dry membrane (kg mol^{-1})
F	Faraday constant (96,487 C mol^{-1})
I	current density (A cm^{-2})
j^i	diffusive mass flux of i phase (kg m^{-2} s^{-1}).
J	Leverett function
K	hydraulic permeability (m^2)
m	mass fraction
M	molecular weight (kg mol^{-1})
n_d	electro-osmotic drag coefficient
P	pressure (Pa)
P_c	capillary pressure (Pa)
RH	inlet relative humidification
R_u	universal gas coefficient (8.314 J mol^{-1} K^{-1})
s_{im}	immobile liquid saturation
s_{int}	interfacial liquid coverage
s_r	reduced liquid saturation
T	temperature (K)
u	fluid velocity and superficial velocity in a porous medium (m s^{-1})

V volume (m^3)

Greek symbols:

γ advection correction factor
δ^i thickness of component i
ε volume fraction of gaseous phase in porous region
θ contact angle (°)
λ membrane water content ($mol_{H_2O}\ mol^{-1}_{SO_3^-}$)
λ^α relative mobility of phase α
μ viscosity ($kg\ m^{-1}\ s^{-1}$)
ν kinematic viscosity ($m^2\ s^{-2}$)
ρ density ($kg\ m^{-3}$)
ρ^{mem} dry membrane density ($kg\ m^{-3}$)
σ surface tension ($N\ m^{-1}$) or electronic conductivity ($S\ m^{-1}$)

Superscripts:

eff effective value in porous region
g gas
l liquid
mem membrane

Subscripts:

GC gas channel
GDL gas diffusion layer
H_2 hydrogen
mem membrane
N_2 nitrogen
O_2 oxygen
pore pore
w water

References

[1] M.P. Manahana, M.C. Hatzella, E.C. Kumburb, M.M. Menchc, Journal of Power Sources 196 (2011) 5573–5582.
[2] Ahmet Turhan, Soowhan Kim, Marta Hatzell, Matthew M. Mench, Electrochimica Acta 55 (2010) 2734–2745.
[3] Hyunchul Ju, Journal of Power Sources 185 (2008) 55–62.
[4] A. Rofaiel, J.S. Eills, P.R. Challa, A. Bazylak, Journal of Power Sources 201 (2012) 219–225.
[5] Joel Pauchet, M. Prat, P. Schott, S. Pulloor Kuttanikkad, International Journal of Hydrogen Energy 37 (2012) 1628–1641.
[6] Jinfeng Wu, Xiao Zi Yuan, Jonathan J. Martin, Haijiang Wang, Jiujun Zhang, Jun Shen, Shaohong Wu, Walter Merida, Journal of Power Sources 182 (2008) 104–119.
[7] Puneet K. Sinha, Chao-Yang Wang, Chemical Engineering Science 63 (2008) 1081–1091.
[8] T.E. Springer, T.A. Zawodinski, S. Gottesfeld, Journal of the Electrochemical Society 136 (1991) 2334–2341.
[9] T.A. Zawodzinski, J. Davey, J. Valerio, S. Gottesfeld, Electrochimica Acta 40 (1995) 297.
[10] S. Motupally, A.J. Becker, J.W. Weidner, Journal of the Electrochemical Society 147 (2000) 3171.
[11] C.Y. Wang, P. Cheng, International Journal of Heat and Mass Transfer 39 (1996) 3607–3618.
[12] M.C. Leverett, AIME Transactions 142 (1941) 152–168.
[13] K.S. Udell, International Journal of Heat and Mass Transfer 28 (1985) 485–495.
[14] J.T. Gostick, M.W. Fowler, M.A. Ioannidis, M.D. Pritzker, Y.M. Volfkovich, A. Sakars, Journal of Power Sources 156 (2006) 375–387.
[15] E.C. Kumbur, K.V. Sharp, M.M. Mench, Journal of the Electrochemical Society 154 (2007) B1305–B1314.
[16] E.C. Kumbur, K.V. Sharp, M.M. Mench, Journal of the Electrochemical Society 154 (2007) B1315–B1324.
[17] X.G. Yang, F.Y. Zhang, A.L. Lubawy, C.Y. Wang, Electrochemical and Solid-State Letters 7 (2004) A408–A411.
[18] F.Y. Zhang, X.G. Yang, C.Y. Wang, Journal of the Electrochemical Society 153 (2006) A225–A232.